environments

Article

The Potential of Waste Phloem Fraction of *Quercus cerris* Bark in Biochar Production

Umut Sen [1,*], Andrei Longo [2], Margarida Gonçalves [2], Isabel Miranda [1] and Helena Pereira [1]

[1] Forest Research Centre, School of Agriculture, University of Lisbon, Tapada da Ajuda, 1349-017 Lisbon, Portugal
[2] Mechanical Engineering and Resource Sustainability Center, Department of Chemistry, Faculty of Sciences and Technology, NOVA University of Lisbon, Campus de Caparica, 2829-516 Caparica, Portugal
* Correspondence: umutsen@isa.ulisboa.pt

Abstract: *Quercus cerris* phloem is a lignocellulosic waste fraction obtained from bark fractionation. Biochars are technologically interesting functional materials that may be produced from lignocellulosic solid materials. This study explores the solid material properties of *Quercus cerris* phloem, evaluates biochar production from it, and explores its application as an adsorbent. In the first part of the study, thermogravimetric analysis, SEM microscopy observations, FT-IR spectroscopy, and ICP-AES analyses were performed on raw *Quercus cerris* phloem. In the second part of the study, biochars and activated carbons were produced and their structure, surface functional groups, methylene blue adsorption properties, and specific surface areas were determined. The results showed that *Quercus cerris* phloem is a lignocellulosic solid material that decomposes in a wide temperature range between 265 and 765 °C. The activation energy of phloem pyrolysis ranged between 82 and 172 kJ mol^{-1} in pyrolysis. The mineral composition is mainly calcium (88%) and potassium (4%). The biochar yield of *Quercus cerris* phloem ranged between 28% and 42% at different moderate temperature–time combinations. Raw phloem, phloem biochars, and phloem-activated carbons show high methylene blue removal efficiencies. Methylene blue adsorption follows pseudo-second-order kinetics. The BET surface areas of *Quercus cerris* phloem-activated carbons varied between 262.1 m^2 g^{-1} and 317.5 m^2 g^{-1}.

Keywords: phloem; *Quercus cerris*; bark; biochar; ICP-AES; TGA

Citation: Sen, U.; Longo, A.; Gonçalves, M.; Miranda, I.; Pereira, H. The Potential of Waste Phloem Fraction of *Quercus cerris* Bark in Biochar Production. *Environments* **2023**, *10*, 71. https://doi.org/10.3390/environments10050071

Academic Editors: Simeone Chianese and Wen-Tien Tsai

Received: 23 February 2023
Revised: 19 April 2023
Accepted: 24 April 2023
Published: 26 April 2023

1. Introduction

Forest wastes are lignocellulosic residues generated by forestry operations that are often left in the forest or combusted to produce industrial or domestic energy. Tree barks are among the important contributors to forestry wastes [1,2] and may attain as high as 400 million cubic meters annually in the world given the approximately 3900 million cubic meters of global wood production in 2020, according to FAO statistics.

Biomass materials have gained interest as renewable energy resources triggered by the depleting of fossil fuels and environmental concerns related to CO_2 emissions from direct combustion of fossil fuels and biomass [3]. Pyrolysis and gasification have received particular attention because they reduce CO_2 emissions and allow production of energy-valuable solid, liquid, and gas products, namely biochars, bio-oils, producer gas, or syngas [4].

Biochars are charcoals produced from biomass via pyrolysis, mostly by slow pyrolysis which is possibly the simplest thermochemical process since it does not require advanced reactors and product separation devices, and produces biochars at low cost and high yield [5]. Biochars are interesting porous solid materials that find applications in different fields such as in soil amendment, in the production of electrode materials, and in the production of activated carbons [6–8].

Extensive research has been carried out into wood and other lignocellulosic materials as raw materials for energy platforms, and into their specific performance in various thermochemical processes [9]. Tree barks have been studied in more recent years and attention has been given to their more complex structural and chemical composition, namely to the fact that they contain two types of cellular tissues, the phloem of lignocellulosic nature and cork, which has suberin as a major structural component [10–12]. The content of cork in barks depends on the species and may be substantial in some species [13]. This is the case for *Quercus cerris* (Turkey oak) which has a bark composed of phloem with substantial cork fractions [14,15].

The valorization of *Q. cerris* bark has been considered targeting the cork fractions, given their commercial value for production of sealants, surfacing, and insulation products [10]. This task requires a trituration of the bark and a fractioning operation that allows a generation of about 27% of cork but also substantial amounts of waste phloem fractions with some cork residual content that require some value-added application in order to contribute to the overall bark valorization [10]. The *Q. cerris* phloem and cork fractions have been analyzed previously to determine chemical composition, anatomical features, and thermochemical degradation [16,17]. Biochars were produced from *Q. cerris* cork and phloem under low-temperature slow pyrolysis/torrefaction conditions (200–350 °C), which showed lignite-like properties, and were considered suitable for soil amendment or adsorbent materials after steam activation [18]. The use of medium or moderate temperatures (400–600 °C) in slow pyrolysis of phloem fractions is still unknown, and it is expected that the phloem properties will affect the biochar production regarding yield, biochar properties, and process efficiency.

This study set out to analyze the phloem waste fraction obtained from *Q. cerris* bark regarding pyrolysis properties and biochar production under moderate-temperature slow pyrolysis conditions. The overall aim is to contribute to the valorization of bark-based forestry wastes since they are widely available, renewable, and sustainable.

2. Materials and Methods

2.1. Materials

Turkey oak (*Quercus cerris*) phloem samples were obtained from the bark of trees from Kahramanmaraş, Turkey, after a pilot-scale mechanical separation. The phloem samples contained some residual cork tissues [10]. Detailed information on the fractionation of the bark can be found in the previous article where the same material as that used in the present study was analyzed [10]. The phloem residues contain 12–23% ash, 5–10% extractives, 3–6% suberin, 32–39% lignin, and 23–45% polysaccharides [16].

In this study, pine cones and pine wood were also analyzed for biochar yield for comparison's sake. The pine cones were collected from *Pinus pinea* trees from Costa de Caparica, Portugal. Pine wood (*Pinus sylvestris*) was obtained from Portugal. A total of one phloem, six biochar, and three phloem-activated carbons were analyzed with two or three replicates as detailed in the following sections.

2.2. Methods

2.2.1. Thermogravimetric Analysis

Pyrolysis experiments on the phloem sample with 250–420 µm particles were conducted using a thermogravimetric analyzer with a differential scanning calorimetry sensor, alumina pans, and a nitrogen flow rate of 55 mL min^{-1}. Approximately 5 mg of phloem was used with the following heating program: isothermal at 40 °C for 5 min; a linear heating step until 800 °C with heating rates of 10, 15, and 30 °C min^{-1}; and a final cooling step of 50 °C min^{-1} [19]. The heat evaluation of the phloem sample was detected by a DSC sensor at a 10 °C min^{-1} heating rate.

2.2.2. Kinetic Analysis of Phloem Pyrolysis

Kinetic analysis of the phloem pyrolysis was carried out first by applying the isoconversional Vyazovkin method [20]. The objective function Ω = φ(Ea) is minimized in three heating rates of 10, 15, and 30 °C min^{-1} [21,22] (Equation (1)).

The temperature integral (I) was calculated using the Senum and Yang approximation (Equations (2) and (3)).

$$\varphi\ (\mathrm{Ea}) = \sum_{i=1}^{n} \sum_{j \neq i}^{n} \frac{\mathrm{I}\ (\mathrm{Ea}, \mathrm{Ta}, \mathrm{i})\ \beta \mathrm{j}}{\mathrm{I}(\mathrm{Ea}, \mathrm{Ta}, \mathrm{j})\ \beta \mathrm{i}} \quad (1)$$

$$\mathrm{I}\ (\mathrm{Ea}, \mathrm{Ta}) = \frac{x^3 + 18\ x^2 + 88x + 96}{x^4 + 20x^3 + 120x^2 + 240x + 120} \quad (2)$$

$$x = \frac{E}{RT} \quad (3)$$

In these equations, i and j represent heating rates, n is the number of heating rates, β is the heating rate (°C min^{-1}), a is the conversion, Ea is the activation energy (J mol^{-1}), R is the universal gas constant (8.314662 J K^{-1} mol^{-1}), and T is the temperature (K).

In addition to the above-mentioned isothermal method, a first-order pseudocomponent model fitting method was also tested to calculate the activation energy and to compare the different kinetic methods [19]. The pseudocomponent model fitting method assumes that biomass chemical components undergo independent parallel degradations during the pyrolysis, and that the overall mass loss is a sum of the mass loss of each pseudocomponent with the following equation:

$$\frac{d\alpha}{dt} = \sum_{i=1}^{n} c_i \times A_i \times\ e^{-\frac{Ea_i}{RT}} \times\ f(\alpha_i) \quad (4)$$

where c_i are biomass fractions and n is the number of pseudocomponents.

2.2.3. FT-IR Analysis

The phloem samples (particles under 180 µm) of *Quercus cerris* were oven-dried at 105 °C during 1 h before experiments. The samples were placed on the diamond (ATR-FTIR) and the reflectance spectra were acquired with a Bruker FT-IR spectrometer in the range of 4000–400 cm^{-1} with a spectral resolution of 4 cm^{-1}.

2.2.4. ICP-AES Analysis

The mineral composition of phloem was evaluated through an Argon ICP-AES (Inductively Coupled Plasma Atomic Emission Spectrometer, Horiba Jobin Yvon, ULTIMA sequential ICP) with a Czerny–Turner monochromator operating at 40.68 MHz. Before the ICP-AES analysis, phloem was combusted at 550 °C until constant weight. The phloem ashes were dissolved in nitric acid (50% *v*/*v*) at 90 °C for 30 min and filtered. The filtrate volume was adjusted to 100 mL with MilliQ water before the ICP-AES analysis.

2.2.5. Calculation of Slagging/Fouling Indices

Predictive slagging/fouling indices were calculated using the mineral oxide percentages of the phloem char ash including Fe_2O_3, CaO, MgO, Na_2O, K_2O, SiO_2, Al_2O_3, and TiO_2 [23,24]. Base-to-acid index (*B*/*A*) was calculated using Equation (5).

$$\frac{B}{A} = \frac{Fe_2O_3 + CaO + MgO + Na_2O + K_2O}{SiO_2 + Al_2O_3 + TiO_2} \quad (5)$$

Silica ratio (*Sr*) was calculated according to Equation (6).

$$Sr = \frac{SiO_2}{SiO_2 + CaO + MgO + Fe_2O_3} * 100 \quad (6)$$

Sintering index (*SI*) was calculated using Equation (7).

$$\mathrm{SI} = \frac{\mathrm{CaO} + \mathrm{MgO}}{\mathrm{Na_2O} + \mathrm{K_2O}} \quad (7)$$

Bed agglomeration index (*BAI*) was calculated using Equation (8).

$$\mathrm{BAI} = \frac{\mathrm{Fe_2O_3}}{\mathrm{Na_2O} + \mathrm{K_2O}} \quad (8)$$

Silica to alumina ratio (*S/A*) was calculated by applying Equation (9).

$$\frac{\mathrm{S}}{\mathrm{A}} = \frac{\mathrm{SiO_2}}{\mathrm{Al_2O_3}} \quad (9)$$

Total alkali content (*TA*) was calculated using Equation (10).

$$\mathrm{TA} = \mathrm{Na_2O} + \mathrm{K_2O} \quad (10)$$

2.2.6. Scanning Electron Microscopy

Scanning electron microscopy (SEM) analyses were performed on phloem and phloem-activated carbon samples using a Hitachi S2400 electron microscope under an accelerating voltage of 20.0 kV.

2.2.7. Moderate Temperature Isothermal Slow Pyrolysis

Slow pyrolysis experiments were conducted isothermally in an oven at temperatures between 400 °C and 600 °C and between 0.5 and 1.5 h residence time. The phloem samples of 420–840 µm were weighed, placed in the oven and sealed to prevent air entrance during the pyrolysis experiments. After the pyrolysis time was over, the samples were cooled in a desiccator, weighed and biochar mass yields were calculated on an as-received basis.

2.2.8. Steam Activation of Phloem Biochars

Activated carbons were produced from the previously produced phloem biochars at 400 °C and 600 °C via steam activation. The biochars were ground down to 180 µm and water-soaked for 1 h (phloem to water mass ratio 1:2 for biochar and deionized water, respectively) and activated under oxygen-lean conditions at 900 °C and 7 min reaction time [18].

2.2.9. Methylene Blue Adsorption

Methylene blue is a cationic dye used in a number of applications in textile, leather, and medical industries [25]. The methylene blue adsorption tests were applied to assess the adsorption ability of the raw phloem, phloem biochars, and phloem activated carbons. Approximately 25 mg of biomass sample was placed in a test tube, and 5 mL of a MB aqueous solution (15 mg/L) was added. The tube was shaken for 3 s (Heidolph REAX top shaker) and the mixture was centrifuged at 5000 rpm for 5 min (Hettich EBA 20) before the adsorption tests for instant (5 min), 24 h, 48 h, 72 h, and 168 h adsorption time. The methylene blue concentration of the dye in the solution was determined using UV–Vis spectrophotometry (Pharmacia LKB-Novaspec II) at 664 nm [18].

2.2.10. Methylene Blue Adsorption Kinetics

Methylene blue adsorption kinetics on raw phloem, phloem biochars, and phloem activated carbons were calculated considering pseudo-first-order and pseudo-second-order kinetics [26].

The pseudo-first-order kinetics (PFO) were calculated using Equation (11).

$$\mathrm{d}q_t/\mathrm{d}_t = k_1 \left(q_e - q_t\right) \quad (11)$$

where q_t and q_e are the amount of dye adsorbed at time t and at equilibrium, and k_1 (h^{-1}) is the pseudo-first-order rate constant.

The pseudo-second-order kinetics (PSO) were calculated using Equation (12).

$$dq_t/d_t = k_2 \left(q_e - q_t\right)\hat{}2 \quad (12)$$

where q_t and q_e are the amount of dye adsorbed at time t and at equilibrium, and k_2 (g mg^{-1} h^{-1}) is the pseudo-first-order rate constant.

2.2.11. BET Surface Area of Activated Carbons

The nitrogen porosimetry analysis of the activated phloem biochar was performed in a Micromeritics porosimeter (model ASAP 2010) at 77 °K, after pre-treatment at 150 °C for at least 12 h. The surface area of activated phloem was determined using the BET model (Brunauer–Emmett–Teller).

2.2.12. Statistical Analysis

A one-way ANOVA test was carried out ($\alpha = 0.05$) to evaluate if there was a significant difference between the biochar yields of *Quercus cerris* phloem under different temperature–time conditions.

3. Results

3.1. Surface Characteristics of Quercus cerris Phloem

The surface of the phloem particles is shown in Figure 1. The surface of the phloem is mainly non-porous (Figure 1a) and it has a high surface roughness (Figure 1b).

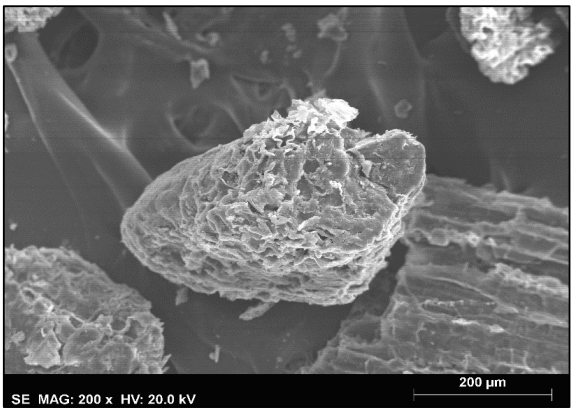

(**a**)

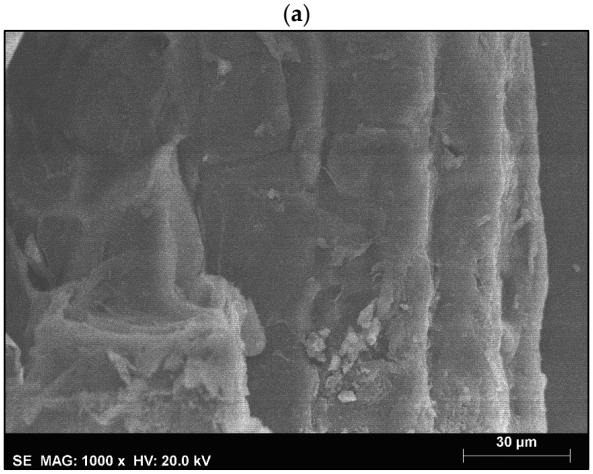

(**b**)

Figure 1. SEM figures of *Quercus cerris* phloem. (**a**) under 200× magnification and (**b**) under 1000× magnification.

The FT-IR analysis results of raw *Quercus cerris* phloem are shown in Figure 2. Three major functional groups are present. The peak at 3600 cm^{-1} is attributed to stretching of O-H groups of moisture and carboxylic acids. The peaks at 2909 and 2842 cm^{-1} are assigned to asymmetric and symmetric C-H vibrations of phloem extractives and of suberin in cork residues, respectively. The intense peak at 1609 cm^{-1} is attributed to C-O stretching of calcium oxalate. The minor peak at 1383 cm^{-1} is assigned to C-H stretch of syringyl lignin, the peak at 1310 cm^{-1} is assigned to C-O stretch in calcium oxalate, and the peak at 1023 cm^{-1} is attributed to C-O stretch of phloem polysaccharides [27]. These surface groups are responsible for the acidic, basic, hydrophobic, or hydrophilic properties (reactivity) of the phloem. The functional groups of phloem biochars and phloem activated carbons are discussed in Section 3.7.

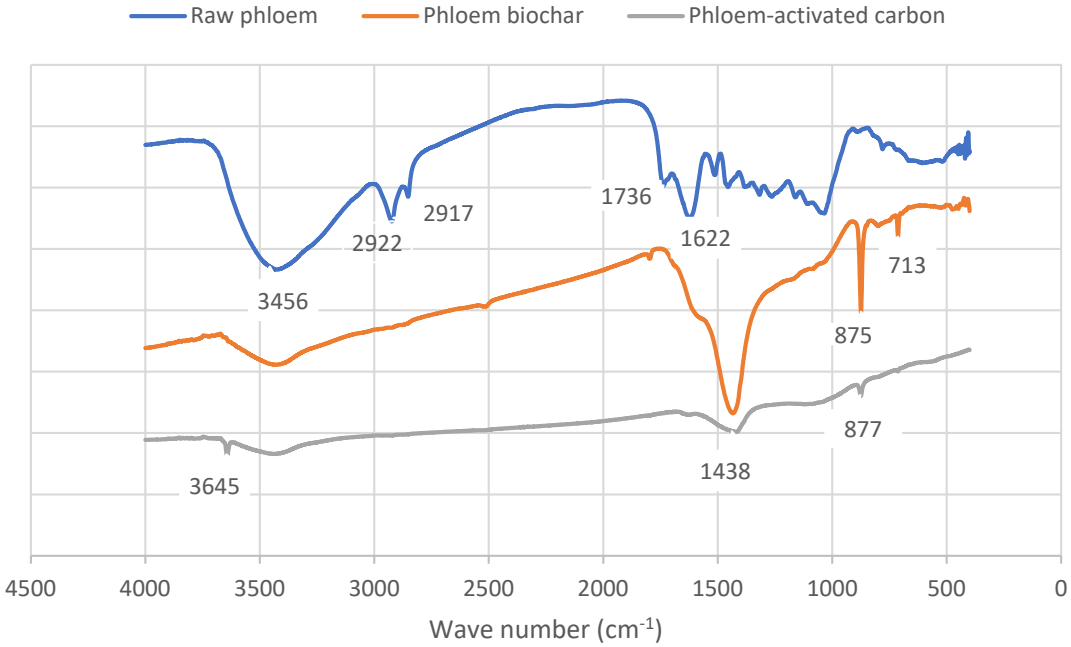

Figure 2. FT-IR spectra of *Quercus cerris* raw phloem, phloem biochar (C50060), and phloem-activated carbon (AC500).

3.2. Mineral Composition of Quercus cerris Phloem

The mineral composition of *Quercus cerris* phloem determined by ICP-AES analysis is shown in Table 1. Calcium is the main element present in the phloem which makes up approximately 88% of all detected minerals. Phloem also contains significant amounts of potassium, magnesium, and iron, and, in lower amounts, aluminum and silicon. A number of trace elements are also present in the phloem including strontium, boron, titanium, and zinc.

Quercus cerris phloem does not contain a high amount of acidic ash components such as aluminum, silicon, and titanium but contains a high amount of basic ash components such as calcium, potassium, iron, etc. These minerals affect the combustion properties of biochars, particularly by creating slagging or fouling problems in combustion systems. The results of the calculated slagging/fouling indices (Table 2) of *Quercus cerris* phloem showed that combustion of phloem or phloem biochars is likely to result in fouling or slagging in the furnace or boilers. On the other hand, ash sintering or bed agglomeration is not predicted.

Table 1. ICP-AES results of phloem ash.

Elements	mg/kg of Phloem Ash	% of Minerals
Al	139.4 ± 12.8	1.37
B	2.5 ± 0.2	0.02
Ba	25.6 ± 1.5	0.25
Ca	8979.9 ± 271.2	88.03
Fe	172.2 ± 2.4	1.69
K	415.7 ± 3.8	4.08
Mg	175.8 ± 10.4	1.72
Mn	71.6 ± 0.4	0.70
Na	56.0 ± 8.0	0.55
Ni	2.5 ± 0.4	0.02
P	36.7 ± 0.7	0.36
Si	95.7 ± 3.2	0.94
Sr	21.1 ± 0.3	0.21
Ti	3.4 ± 0.1	0.03
Zn	3.4 ± 1.6	0.03
Total	10,201.5	

Table 2. Predictive slagging/fouling indices of *Quercus cerris* phloem.

Index		Slagging/Fouling Potential
Base to acid (B/A)	28.86	Severe slagging [28]
Silica ratio (Sr)	1.54	High slagging [28]
Sintering (SI)	22.31	Sintering not likely [29]
Bed agglomeration (BAI)	0.43	Bed agglomeration not likely [28]
Silica to alumina (S/A)	0.78	High slagging/fouling [24]
Total alkali (TA)	4.00	High slagging/fouling [24]

3.3. Pyrolysis Behavior and Kinetics of Quercus cerris Phloem

The pyrolysis of *Quercus cerris* phloem shows typical lignocellulosic thermal degradation (Figure 3). Significant mass loss starts at approximately 280 °C with a fast devolatilization until 370 °C and then becomes slower until 600 °C [30]. The char oxidation reaction occurs between 475 °C and 665 °C.

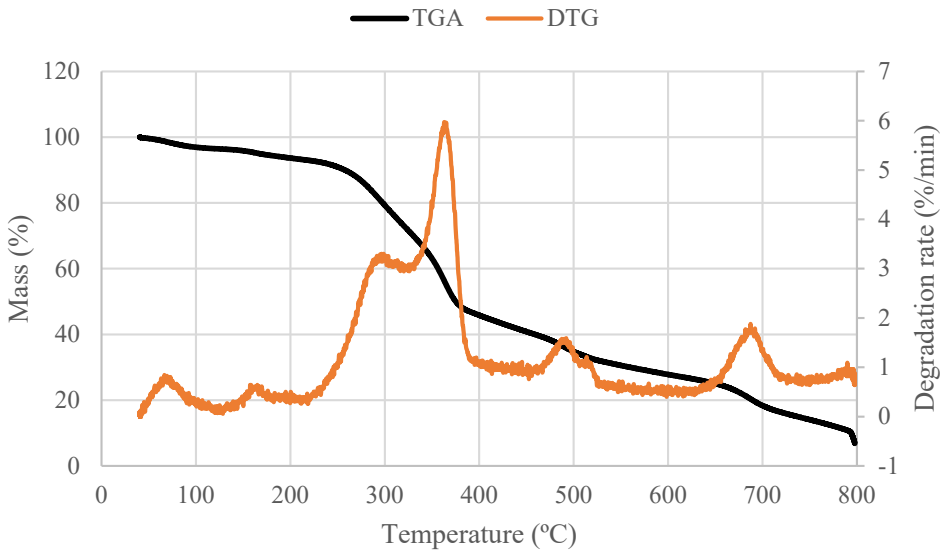

Figure 3. Pyrolysis behavior of phloem samples (heating rate: 10 °C/min).

The heat flow of phloem pyrolysis proceeds as an endothermal process until char oxidation and later becomes exothermic which renders the overall reaction exothermic (Figure 4).

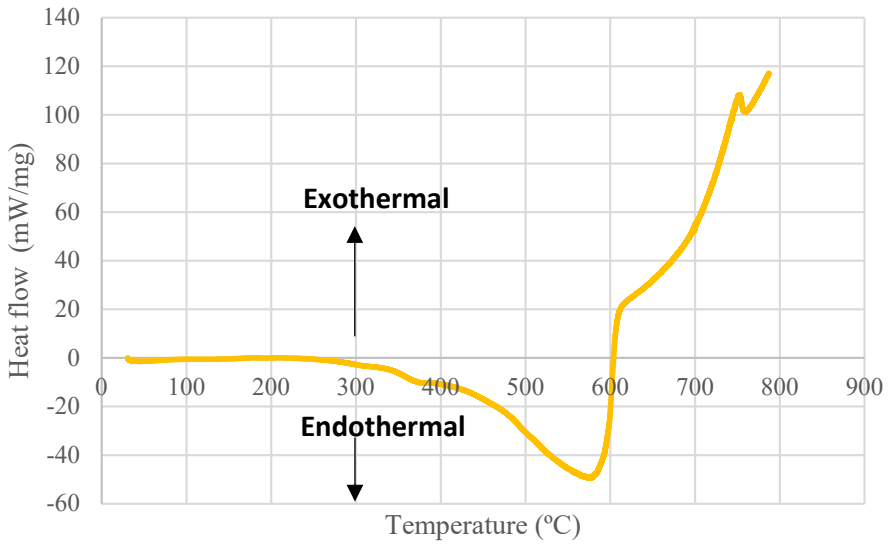

Figure 4. Heat flow profile of *Quercus cerris* phloem during pyrolysis determined by a DSC sensor (heating rate: 10 °C/min).

The kinetic analysis of phloem pyrolysis by the Vyazovkin method showed that phloem has an activation energy of approximately 172 kJ mol^{-1}. The activation energy calculated by Vyazovkin method shows that phloem is stable until 65% of conversion (520 °C) with an average activation energy of 170 kJ mol^{-1} which corresponds to its main devolatilization range. After that conversion, the activation energy increases up to 210 kJ mol^{-1} in the char oxidation step (Figure 5). The pseudocomponent model fitting resulted in an activation energy of 82 kJ mol^{-1} which was approximately half of the isoconversional value. The fitting of the data was good (Figure 6) implying that the results of the applied kinetic methods vary.

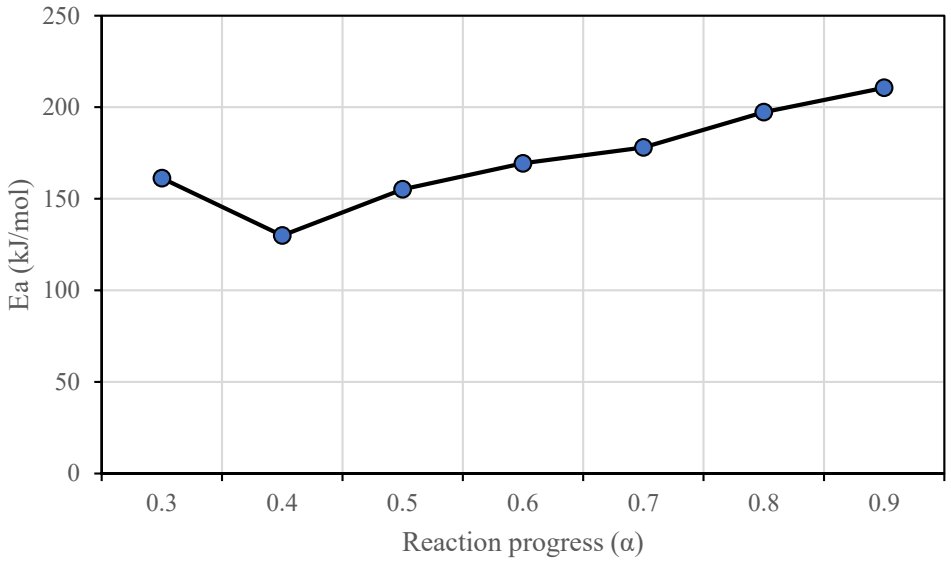

Figure 5. Variation of the activation energy of phloem calculated by the Vyazovkin method.

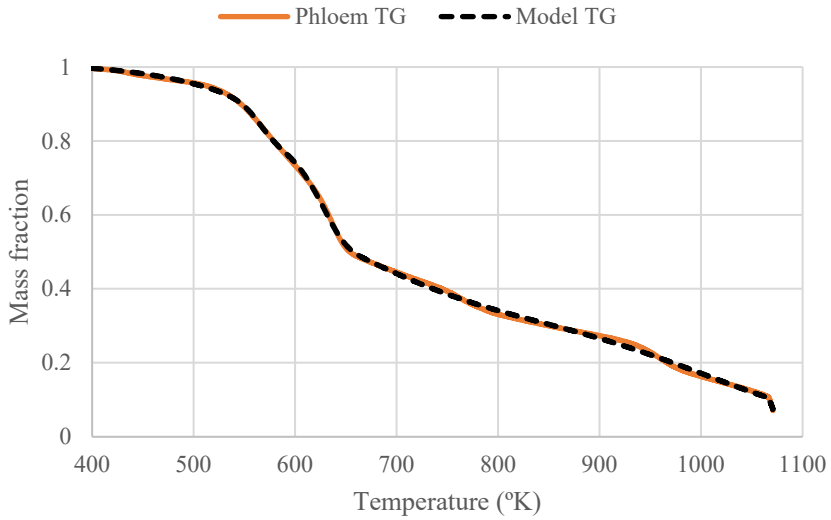

Figure 6. First-order pseudocomponent model fitting of phloem pyrolysis (heating rate: 10 °C/min).

3.4. Biochar Yield

Moderate-temperature slow pyrolysis of *Quercus cerris* phloem results in approximately 29–42% biochars at temperatures between 400 and 600 °C (Figure 7a). The biochar yield decreases considerably when the pyrolysis temperature is increased from 400 °C to 500 °C. On the other hand, at 600 °C, *Quercus cerris* phloem still produces approximately 30% biochar. The biochar yield was similar between 30 min and 60 min pyrolysis time (approximately 33%) at 500 °C but it reduces to 28% when the pyrolysis time is extended to 150 min (Figure 7b). Interestingly, *Quercus cerris* phloem results in higher biochar yield than other forest residues (pine cones) and pine wood (Figure 5c). The high biochar yield of phloem is a promising factor in the economic evaluation of bark-based lignocellulosic wastes. The one-way ANOVA test revealed that there was no significant difference in biochar yields of *Quercus cerris* phloem between the different pyrolysis temperature–time conditions.

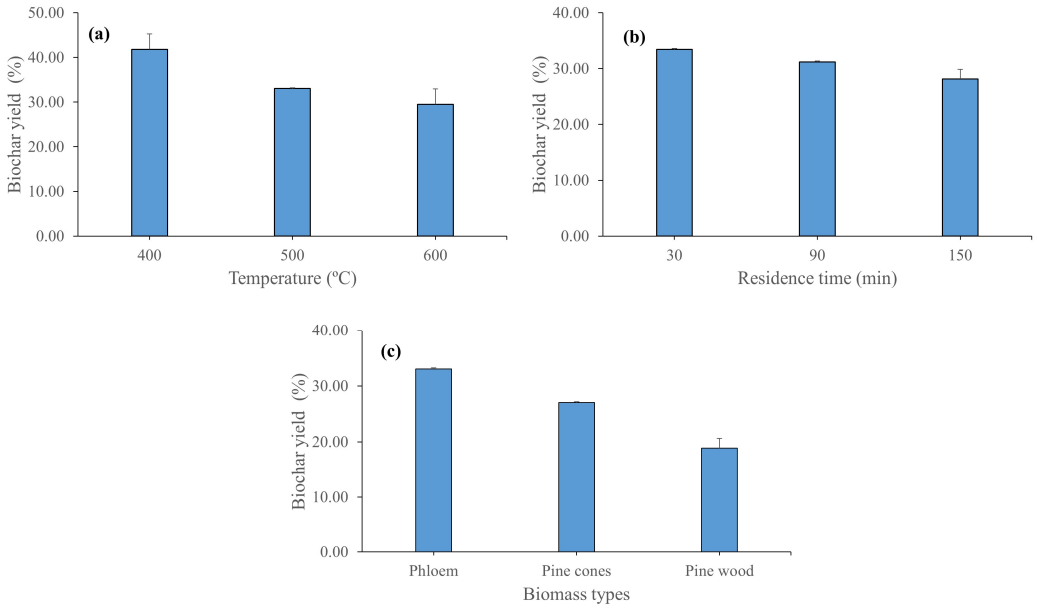

Figure 7. Biochar yields after moderate temperature pyrolysis of *Quercus cerris* phloem: (**a**) comparison of biochar yields at different temperatures (residence time: 60 min), (**b**) comparison of biochar yields at different residence times (final pyrolysis temperature: 500 °C), and (**c**) comparison of biochar yields of *Quercus cerris* phloem with pine cones and pine wood (final pyrolysis temperature: 500 °C).

3.5. Methylene Blue Adsorption

Biochars are frequently used as adsorbent materials to remove dyes, heavy metals, or other pollutants from water. Methylene blue is a basic dye used to assess the dye adsorption capacity of different solid materials. The results of the dye adsorption capacity of raw phloem and phloem biochars are shown in Figures 8 and 9. The results demonstrate that untreated phloem is a better adsorbent of methylene blue with the shorter contact times but later, after 1 week, biochars surpass the removal efficiency by reaching 91–99% removal (Figure 8). Biochars exposed to a higher temperature during pyrolysis showed better methylene blue removal efficiency while the pyrolysis time did not show a significant effect on methylene blue removal.

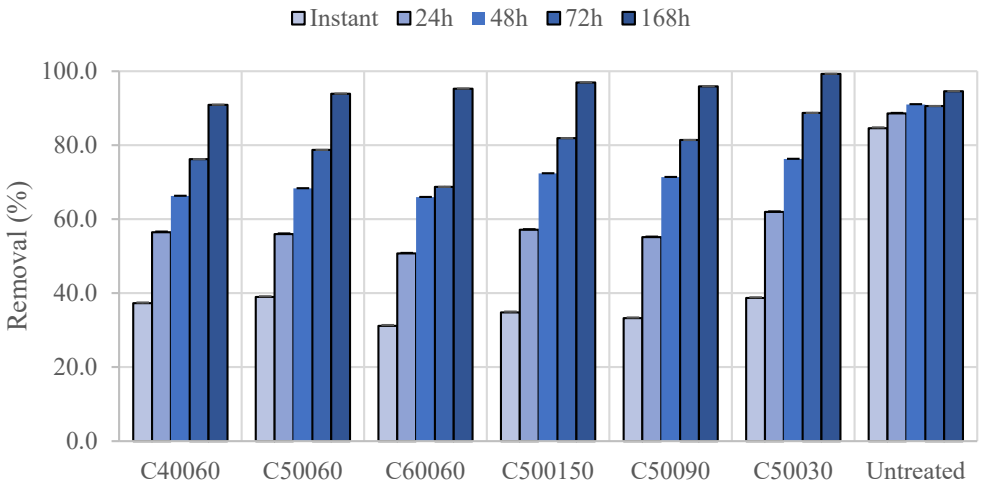

Figure 8. Methylene blue removal efficiencies of *Quercus cerris* phloem and chars produced under different conditions: Untreated—raw phloem; C40060—char produced at 400 °C and 60 min residence time; C50060—char produced at 500 °C and 60 min residence time; C60060—char produced at 600 °C and 60 min residence time; C500150—char produced at 500 °C and 150 min residence time; C50090—char produced at 500 °C and 90 min residence time; C50030—char produced at 500 °C and 30 min residence time.

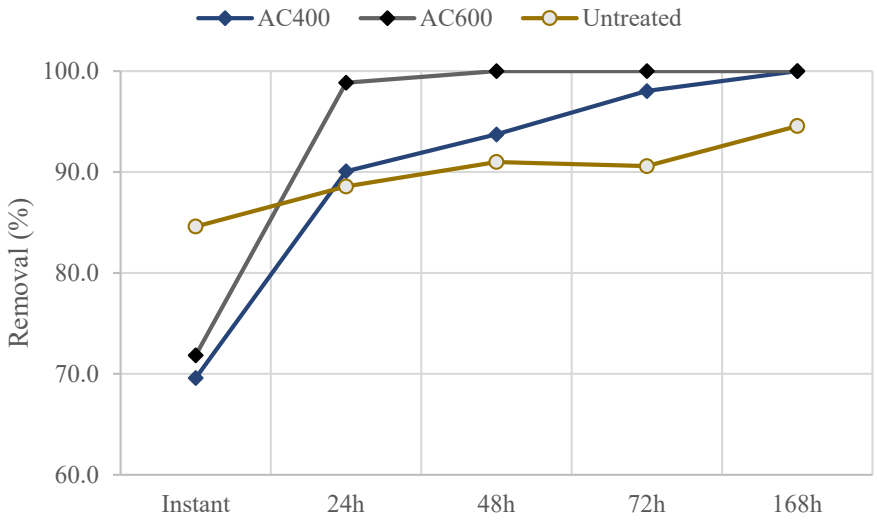

Figure 9. Methylene blue removal efficiencies of *Quercus cerris* phloem and activated carbons: Untreated—untreated phloem; AC400—activated carbon produced from C40060 phloem biochar; AC600—activated carbon produced from C60060 phloem biochar.

Interestingly, the activated carbons produced from phloem also showed lower methylene blue removal efficiencies than raw phloem for short contact time, but after 1 day they already showed better methylene blue removal. The phloem-activated carbons reached a total removal of methylene blue after 1 week compared to 94% removal of raw phloem (Figure 9).

The adsorption of methylene blue on phloem biochars and phloem-activated carbons followed pseudo-first-order and pseudo-second-order kinetic models (Table 3). The pseudo-second-order better described the methylene blue adsorption with greater R^2 values.

Table 3. Pseudo-first-order and pseudo-second-order kinetics of methylene blue adsorption of *Quercus cerris* phloem, biochars, and activated carbons.

Biomass	C40060	C50060	C60060	C500150	C50090	C50030	AC400	AC600	Untreated
k_1	0.0126	0.0152	0.0167	0.0194	0.0179	0.0282	0.0454	0.1603	0.0058
R^2	0.93	0.96	0.97	0.98	0.98	0.99	0.88	0.93	0.93
k_2	0.5365	0.0258	0.6663	0.4491	0.4739	0.3515	0.0719	0.0040	0.0070
R^2	0.98	0.98	0.95	0.98	0.98	0.98	0.99	0.99	0.99

3.6. BET Surface Area of Activated Carbons

The surface area of activated carbons is among the most important parameters in adsorption and in the production of electrode materials from biochars. The results showed that the BET surface area of phloem-activated carbon produced from biochars pyrolyzed at 400 ° is 262.1 $m^2\ g^{-1}$ while the surface area of phloem-activated carbon produced from biochars pyrolyzed at 600 °C is 317.5 $m^2\ g^{-1}$ (Table 4). These results indicate that steam activation was efficient. The nitrogen adsorption isotherms of phloem-activated carbons were similar and showed type IV adsorption isotherms according to the IUPAC classification (Figure 10).

Table 4. Pore properties of phloem-activated carbons.

Activated Carbons	AC400	AC600
BET surface area ($m^2\ g^{-1}$)	262.1	317.5
Total pore volume (BJH adsorption, $cm^3\ g^{-1}$)	0.04	0.05
Total pore volume (BJH desorption, $cm^3\ g^{-1}$)	0.04	0.04
Total pore volume at adsorption ($p/p^\circ = 0.99$, $cm^3\ g^{-1}$)	0.14	0.16
Total pore volume at desorption ($p/p^\circ = 0.99$, $cm^3\ g^{-1}$)	0.14	0.16
Average pore width (BJH adsorption, nm)	19.02	6.77
Average pore width (BJH desorption, nm)	36.34	7.93
Average pore diameter (4V/A by BET adsorption, nm)	2.12	2.02
Average pore diameter (4V/A by BET desorption, nm)	2.12	2.02

3.7. Surface Characteristics of Biochars and Activated Carbons

The surface groups of the phloem biochars and phloem-activated carbons are shown in Figure 9. The phloem biochars retained their structure after the pyrolysis. They contained cork impurities and calcium carbonate crystals (Figure 11a). Interestingly, pits between the phloem cells did not alter their structure (Figure 11b) and possibly play a role in the activation of phloem biochars. The phloem-activated carbons, on the other hand, were

subject to thermal degradation (Figure 11c,d). The mineral content of the phloem remained in the activated carbons which were mostly calcite (sharp-edged smaller particles with light colour) and silica (a large amorphous particle with light colour) (Figure 11c). The steam activation created micropores in the phloem particles (Figure 11d).

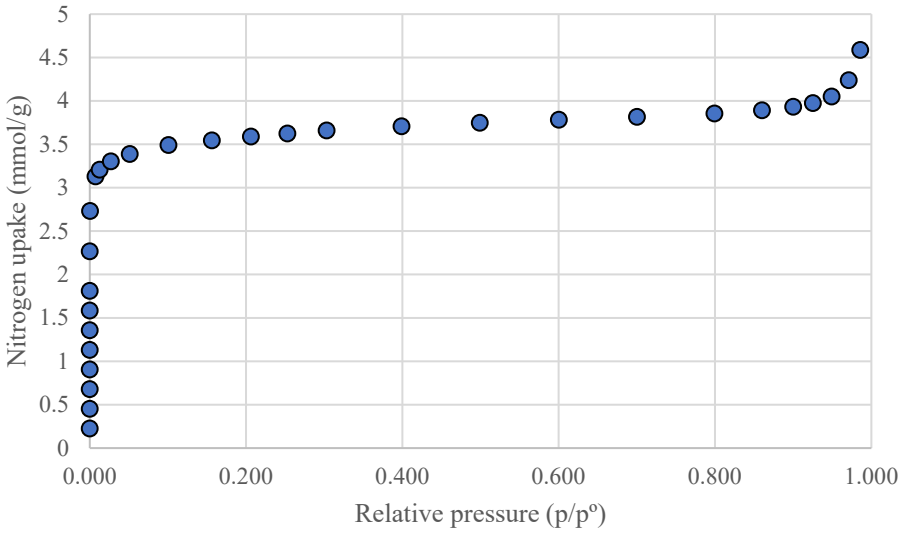

Figure 10. Nitrogen adsorption isotherm of phloem-activated carbon AC600.

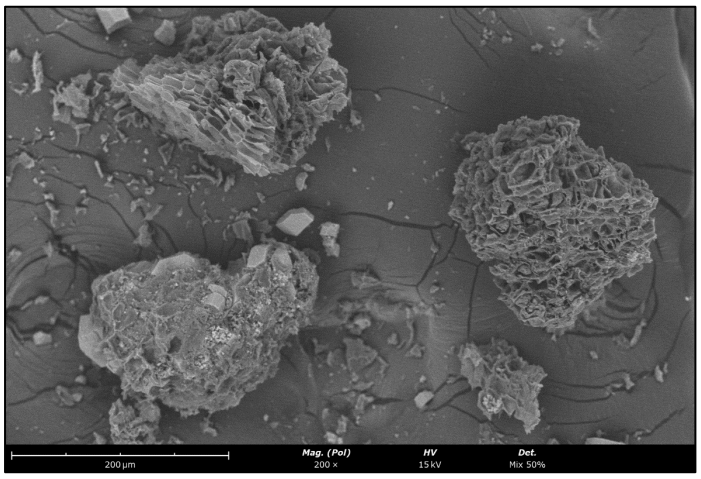

(**a**)

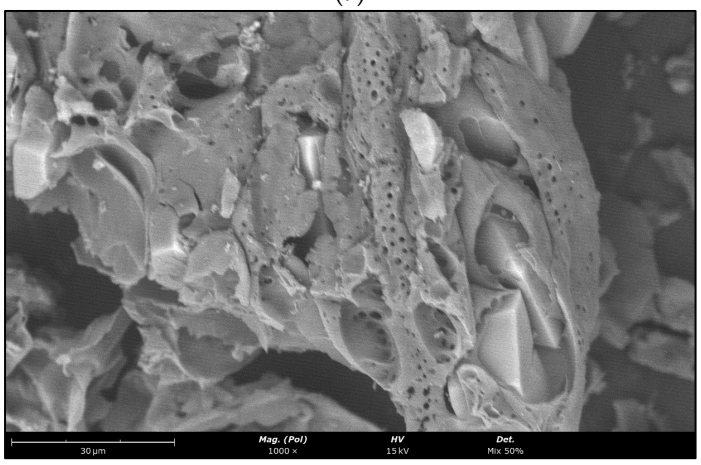

(**b**)

Figure 11. *Cont.*

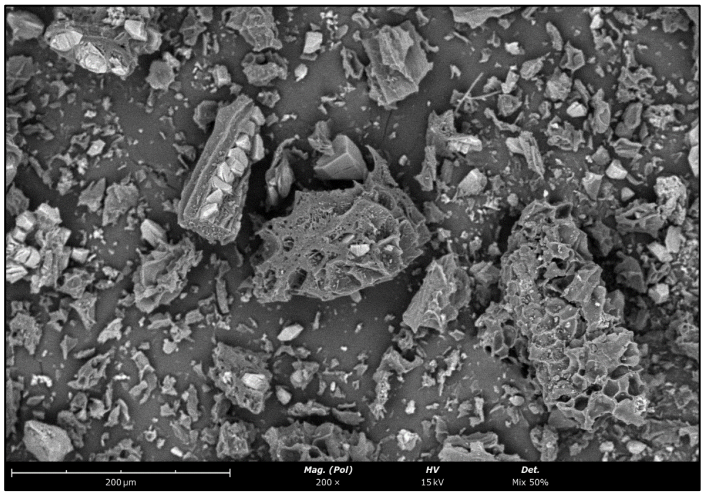

(**c**)

(**d**)

Figure 11. Surface structure of phloem biochars (C50060, (**a**,**b**)) and phloem-activated carbons (AC500, (**c**,**d**)).

The FT-IR results (Figure 2) of phloem biochars and phloem-activated carbon showed that the O-H stretch at 3456 cm^{-1} decreased in the biochars and phloem-activated carbons which is linked with the loss of moisture. The C=O and C-O stretching bands at 1736 cm^{-1} and 1622 cm^{-1} also decreased in biochars, implying that residual suberin and phloem polysaccharides underwent degradation during moderate-temperature slow pyrolysis. In phloem biochars, three additional peaks appeared after biochar production at 1438 cm^{-1}, 875 cm^{-1}, and 713 cm^{-1}. These peaks had already decreased in intensity after activated carbon production and were assigned to calcium carbonate (calcite) which is possibly formed after CO release from calcium oxalate minerals of phloem during the pyrolysis.

4. Discussion

Quercus cerris phloem is a lignocellulosic solid waste with high ash content that is obtained in high amounts during bark fractionation for cork retrieval [16]. The thermogravimetric analysis showed that phloem degrades in a wide range of temperatures possibly because of its high lignin content [14]. Lignin is known to be highly stable at elevated temperatures [31,32]. The heat flow profile of *Quercus cerris* phloem suggests that lignin and hemicelluloses degradation becomes significant in the high-temperature range since the pyrolysis of these components is reported to be exothermic [33]. It is possible that charring reactions of cellulose also contribute to the exothermicity of the reaction [34]. Interestingly, the exothermicity of phloem pyrolysis is similar to that of cork [35]. These results imply

that pyrolysis behavior of different barks could be modeled using cork and phloem as representative components. The activation energy of phloem is variable and ranged most likely between 72 kJ mol^{-1} and 172 kJ mol^{-1}. The variable activation energy of phloem at different conversions indicates that it is a multi-step process [36], which is in agreement with the thermogravimetric results and the chemical analyses.

The surface of the phloem has high roughness and contains acidic and basic surface functional groups which are subject to thermal degradation or alteration during pyrolysis. The surface features of the phloem surface make it a favorable material for biochar production because micropores and mesopores are likely to develop from these surfaces during pyrolysis. The porous surface of biochars was shown to be important in soil amendment or adsorbent applications [37,38].

The ash of *Quercus cerris* phloem is mainly composed of calcium followed by potassium, magnesium, and iron. The high calcium content is a distinct feature of barks and *Quercus cerris* bark contains calcium in the upper reported range [23]. Small amounts of trace elements are also present.

Biochar production from *Quercus cerris* phloem seems to be a promising path not only for reducing the waste content but also for producing functional biochars. A moderate temperature pyrolysis is required to produce the biochars. The utilization potential of phloem for biochar production requires an estimation of biochar yields. The biochar yields of *Quercus cerris* phloem ranged between 28% and 42% under moderate-temperature (400–600 °C) conditions. Higher temperatures and residence times reduce the biochar yield (Figure 12). It should be noted that these values are valid only for small sample sizes. More experiments are needed to evaluate the biochar yield from other *Quercus cerris* phloem materials and from phloem of other species.

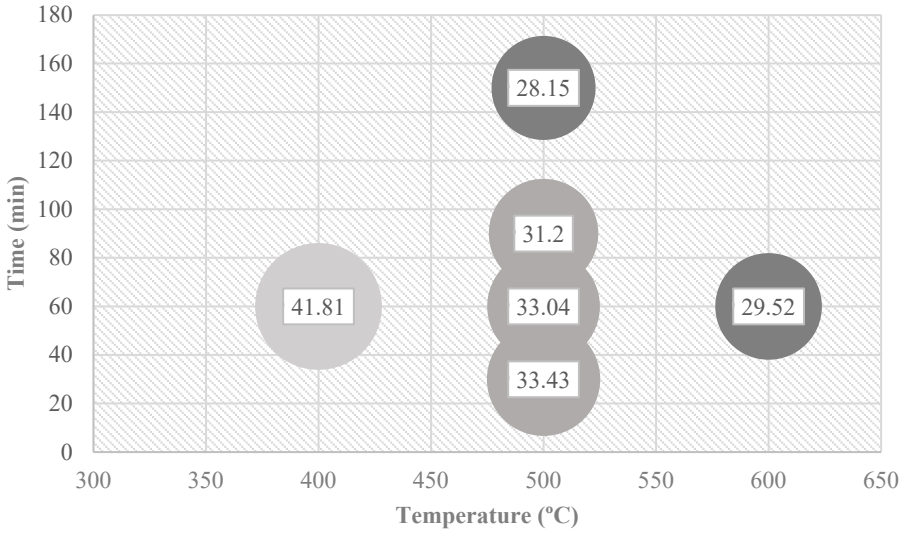

Figure 12. Comparison of biochar yields (% inside the bubble) of *Quercus cerris* phloem obtained with different time–temperature conditions.

Biochars have a wide range of utilizations including solid fuels, soil amendment materials, adsorbents, and activated carbon precursors [37]. The fuel uses of raw phloem and phloem chars should be undertaken with caution as the mineral oxides in the phloem are likely to create slagging or fouling problems in the combustors. Soil amendment seems to be a viable route for phloem biochars as they become carbon-rich after the pyrolysis devolatilization. The mineral content of phloem also suggests soil amendment applications considering its potassium and calcium content. It should also be noted that phloem biochars cannot be considered as fertilizers alone due to their low content of nitrogen [39]. Raw phloem and biochars have low surface area but they may be used as adsorbents because they have surface active groups which are likely to play a role in chemisorption [40]. The

high methylene blue adsorption of raw phloem and phloem biochars is encouraging and occurs close to the adsorption of activated carbons [18]. These solid materials might be applied to remove cationic dyes or heavy metals in low concentrations [41,42]. In fact, one of the most interesting applications of natural adsorbents is in removing pollutants in low concentrations because they are low-cost and efficient [25,43].

The production of activated carbons is perhaps the most interesting path in the valorization of waste phloem as they can be used both as adsorbents or as electrode materials [44]. A single-step steam activation seems to be efficient in producing activated carbons with comparable specific surface areas from phloem with other lignocellulosic materials activated chemically [45]. The activated carbons showed total removal of methylene blue which validated their efficiency. It is possible that the heterogeneous structure of phloem biochars and the presence of residual cork in the samples affect the adsorption efficiency [18]. It is also likely that steam activation also contributes to methylene blue adsorption by creating surface oxygen groups. The methylene blue removal by the activated carbons fitted well with pseudo-second-order kinetics implying that the rate-limiting step is chemisorption and that liquid film diffusion, surface adsorption, and intra-particle diffusion coexist in the adsorption [46,47]. The pseudo-second-order kinetics better described the methylene blue adsorption with greater R^2 values. This result is in agreement with previous reports on methylene blue adsorption on biochars [41,48].

5. Conclusions

The following conclusions can be derived from this study:

1. *Quercus cerris* phloem is a renewable and sustainable lignocellulosic solid material, that may have various valorization pathways.
2. The ash content of *Quercus cerris* phloem is high and composed mainly of calcium (88%) and potassium (4%) which are likely to cause slagging and fouling problems in combustion.
3. *Quercus cerris* phloem decomposes in a wide temperature range between 265 °C and 765 °C.
4. The activation energy of *Quercus cerris* phloem pyrolysis ranges between 82 kJ mol^{-1} and 172 kJ mol^{-1}.
5. The biochar yield of *Quercus cerris* phloem under moderate temperatures (400–600 °C) ranges between 28% and 42%.
6. Raw *Quercus cerris* phloem, phloem biochars, and phloem-activated carbons show high methylene blue removal efficiencies. Methylene blue adsorption follows pseudo-second-order kinetics.
7. The specific surface area of *Quercus cerris* phloem-activated carbons ranged between 262 m^2 g^{-1} and 318 m^2 g^{-1} indicating that the steam activation was efficient.

Author Contributions: U.S., M.G. and H.P.; methodology, A.L.; investigation, U.S. and I.M.; resources, U.S. and M.G.; data curation, U.S.; writing—original draft preparation, U.S.; writing—review and editing, M.G, I.M. and H.P.; visualization, H.P.; supervision. All authors have read and agreed to the published version of the manuscript.

Funding: This work has been supported by FCT—Fundação para a Ciência e Tecnologia within the R&D Units Project Scope: Mechanical Engineering and Resource Sustainability Center, MEtRICs (UIDP/04077/2020) and by Forest Research Centre, CEF, (UIDB/00239/2020). A.U. Sen acknowledges support from FCT through a research contract (DL 57/2016).

Data Availability Statement: Not applicable.

Acknowledgments: The authors thank Nuno Costa and Carla Rodrigues from LAQV Requimte of NOVA University of Lisbon for ICP-AES and nitrogen porosimetry determinations, Professor Francisco Lemos from Instituto Superior Técnico for thermogravimetric analysis, and Isabel Nogueira from Instituto Superior Técnico for scanning electron microscopy analysis.

Conflicts of Interest: The authors declare no conflict of interest.

References

1. Pasztory, Z.; Mohácsiné, I.R.; Gorbacheva, G.; Börcsök, Z. The Utilization of Tree Bark. *BioResources* **2016**, *11*, 7859–7888. [CrossRef]
2. Feng, S.; Cheng, S.; Yuan, Z.; Leitch, M.; Xu, C. Valorization of bark for chemicals and materials: A review. *Renew. Sustain. Energy Rev.* **2013**, *26*, 560–578. [CrossRef]
3. Moriarty, P.; Honnery, D. What Is the Global Potential for Renewable Energy? *Renew. Sustain. Energy Rev.* **2012**, *16*, 244–252. [CrossRef]
4. Brewer, C.E.; Schmidt-Rohr, K.; Satrio, J.A.; Brown, R.C. Characterization of Biochar from Fast Pyrolysis and Gasification Systems. *Environ. Prog. Sustain. Energy Off. Publ. Am. Inst. Chem. Eng.* **2009**, *28*, 386–396. [CrossRef]
5. Şen, A.U.; Pereira, H. State-of-the-Art Char Production with a Focus on Bark Feedstocks: Processes, Design, and Applications. *Processes* **2021**, *9*, 87. [CrossRef]
6. Lehmann, J.; Kuzyakov, Y.; Pan, G.; Ok, Y.S. Biochars and the Plant-Soil Interface. *Plant Soil* **2015**, *395*, 1–5. [CrossRef]
7. Huggins, T.; Wang, H.; Kearns, J.; Jenkins, P.; Ren, Z.J. Biochar as a Sustainable Electrode Material for Electricity Production in Microbial Fuel Cells. *Bioresour. Technol.* **2014**, *157*, 114–119. [CrossRef]
8. Tan, X.; Liu, S.; Liu, Y.; Gu, Y.; Zeng, G.; Hu, X.; Wang, X.; Liu, S.; Jiang, L. Biochar as Potential Sustainable Precursors for Activated Carbon Production: Multiple Applications in Environmental Protection and Energy Storage. *Bioresour. Technol.* **2017**, *227*, 359–372. [CrossRef]
9. Bridgwater, T. Biomass for Energy. *J. Sci. Food Agric.* **2006**, *86*, 1755–1768. [CrossRef]
10. Şen, A.; Leite, C.; Lima, L.; Lopes, P.; Pereira, H. Industrial Valorization of *Quercus cerris* Bark: Pilot Scale Fractionation. *Ind. Crops Prod.* **2016**, *92*, 42–49. [CrossRef]
11. Miranda, I.; Gominho, J.; Mirra, I.; Pereira, H. Chemical Characterization of Barks from Picea Abies and Pinus Sylvestris after Fractioning into Different Particle Sizes. *Ind. Crops Prod.* **2012**, *36*, 395–400. [CrossRef]
12. Ferreira, J.P.A.; Miranda, I.; Gominho, J.; Pereira, H. Selective Fractioning of Pseudotsuga Menziesii Bark and Chemical Characterization in View of an Integrated Valorization. *Ind. Crops Prod.* **2015**, *74*, 998–1007. [CrossRef]
13. Leite, C.; Pereira, H. Cork-Containing Barks—A Review. *Front. Mater.* **2017**, *3*, 63. [CrossRef]
14. Şen, A.; Miranda, I.; Santos, S.; Graça, J.; Pereira, H. The Chemical Composition of Cork and Phloem in the Rhytidome of *Quercus cerris* Bark. *Ind. Crops Prod.* **2010**, *31*, 417–422. [CrossRef]
15. Şen, A.; Quilhó, T.; Pereira, H. Bark Anatomy of *Quercus cerris* L. Var. Cerris from Turkey. *Turk. J. Bot.* **2011**, *35*, 45–55. [CrossRef]
16. Sen, A.; Miranda, I.; Esteves, B.; Pereira, H. Chemical Characterization, Bioactive and Fuel Properties of Waste Cork and Phloem Fractions from *Quercus cerris* L. Bark. *Ind. Crops Prod.* **2020**, *157*, 112909. [CrossRef]
17. Şen, A.; Quilhó, T.; Pereira, H. The Cellular Structure of Cork from *Quercus cerris* Var. Cerris Bark in a Materials' Perspective. *Ind. Crops Prod.* **2011**, *34*, 929–936. [CrossRef]
18. Şen, A.U.; Nobre, C.; Durão, L.; Miranda, I.; Pereira, H.; Gonçalves, M. Low-Temperature Biochars from Cork-Rich and Phloem-Rich Wastes: Fuel, Leaching, and Methylene Blue Adsorption Properties. *Biomass Convers. Biorefin.* **2020**, *12*, 3899–3909. [CrossRef]
19. Şen, A.U.; Fonseca, F.G.; Funke, A.; Pereira, H.; Lemos, F. Pyrolysis Kinetics and Estimation of Chemical Composition of *Quercus cerris* Cork. *Biomass Convers. Biorefin.* **2020**, *12*, 4835–4845. [CrossRef]
20. Şen, U.; Pereira, H. Pyrolysis Behavior of Alternative Cork Species. *J. Therm. Anal. Calorim.* **2022**, *147*, 4017–4025. [CrossRef]
21. Vyazovkin, S. Evaluation of Activation Energy of Thermally Stimulated Solid-state Reactions under Arbitrary Variation of Temperature. *J. Comput. Chem.* **1997**, *18*, 393–402. [CrossRef]
22. Vyazovkin, S.; Wight, C.A. Model-Free and Model-Fitting Approaches to Kinetic Analysis of Isothermal and Nonisothermal Data. *Thermochim. Acta* **1999**, *340*, 53–68. [CrossRef]
23. Fengel, D.; Wegener, G. Wood: Chemistry, Ultrastructure. *Reactions* **1984**, *613*, 1960–1982.
24. Ovčačíková, H.; Velička, M.; Vlček, J.; Topinková, M.; Klárová, M.; Burda, J. Corrosive Effect of Wood Ash Produced by Biomass Combustion on Refractory Materials in a Binary Al–Si System. *Materials* **2022**, *15*, 5796. [CrossRef]
25. Oraon, A.; Prajapati, A.K.; Ram, M.; Saxena, V.K.; Dutta, S.; Gupta, A.K. Synthesis, Characterization, and Application of Microporous Biochar Prepared from Pterospermum Acerifolium Plant Fruit Shell Waste for Methylene Blue Dye Adsorption: The Role of Surface Modification by SDS Surfactant. *Biomass Convers. Biorefin.* **2022**, 1–23. [CrossRef]
26. Chowdhury, S.; Saha, P. Adsorption Kinetic Modeling of Safranin onto Rice Husk Biomatrix Using Pseudo-first-and Pseudo-second-order Kinetic Models: Comparison of Linear and Non-linear Methods. *CLEAN–Soil Air Water* **2011**, *39*, 274–282. [CrossRef]
27. Sen, A.; Marques, A.V.; Gominho, J.; Pereira, H. Study of Thermochemical Treatments of Cork in the 150–400 °C Range Using Colour Analysis and FTIR Spectroscopy. *Ind. Crops Prod.* **2012**, *38*, 132–138. [CrossRef]
28. Lachman, J.; Baláš, M.; Lisý, M.; Lisá, H.; Milčák, P.; Elbl, P. An Overview of Slagging and Fouling Indicators and Their Applicability to Biomass Fuels. *Fuel Process. Technol.* **2021**, *217*, 106804. [CrossRef]
29. Llorente, M.J.F.; García, J.E.C. Comparing Methods for Predicting the Sintering of Biomass Ash in Combustion. *Fuel* **2005**, *84*, 1893–1900. [CrossRef]
30. Şen, A.; Van Den Bulcke, J.; Defoirdt, N.; Van Acker, J.; Pereira, H. Thermal Behaviour of Cork and Cork Components. *Thermochim. Acta* **2014**, *582*, 94–100. [CrossRef]
31. Fang, Z.; Sato, T.; Smith, R.L., Jr.; Inomata, H.; Arai, K.; Kozinski, J.A. Reaction Chemistry and Phase Behavior of Lignin in High-Temperature and Supercritical Water. *Bioresour. Technol.* **2008**, *99*, 3424–3430. [CrossRef] [PubMed]

32. Song, P.; Cao, Z.; Fu, S.; Fang, Z.; Wu, Q.; Ye, J. Thermal degradation and flame retardancy properties of ABS/lignin: Effects of lignin content and reactive compatibilization. *Thermochim. Acta* **2011**, *518*, 59–65. [CrossRef]
33. Yang, H.; Yan, R.; Chen, H.; Lee, D.H.; Zheng, C. Characteristics of Hemicellulose, Cellulose and Lignin Pyrolysis. *Fuel* **2007**, *86*, 1781–1788. [CrossRef]
34. Ball, R.; McIntosh, A.C.; Brindley, J. Feedback Processes in Cellulose Thermal Decomposition: Implications for Fire-Retarding Strategies and Treatments. *Combust. Theory Model.* **2004**, *8*, 281. [CrossRef]
35. Sen, U.; Martins, M.; Santos, E.; Lemos, M.A.; Lemos, F.; Pereira, H. Slow Pyrolysis of *Quercus cerris* Cork: Characterization of Biochars and Pyrolysis Volatiles. *Environments* **2023**, *10*, 4. [CrossRef]
36. Vyazovkin, S. A Time to Search: Finding the Meaning of Variable Activation Energy. *Phys. Chem. Chem. Phys.* **2016**, *18*, 18643–18656. [CrossRef] [PubMed]
37. Qian, K.; Kumar, A.; Zhang, H.; Bellmer, D.; Huhnke, R. Recent Advances in Utilization of Biochar. *Renew. Sustain. Energy Rev.* **2015**, *42*, 1055–1064. [CrossRef]
38. Leng, L.; Xiong, Q.; Yang, L.; Li, H.; Zhou, Y.; Zhang, W.; Jiang, S.; Li, H.; Huang, H. An overview of engineering the surface area and porosity of biochar. *Sci. Total Environ.* **2021**, *763*, 144204. [CrossRef]
39. Carrier, M.; Hardie, A.G.; Uras, Ü.; Görgens, J.; Knoetze, J.H. Production of Char from Vacuum Pyrolysis of South-African Sugar Cane Bagasse and Its Characterization as Activated Carbon and Biochar. *J. Anal. Appl. Pyrolysis* **2012**, *96*, 24–32. [CrossRef]
40. Chojnacka, K.; Chojnacki, A.; Gorecka, H. Biosorption of Cr^{3+}, Cd^{2+} and Cu^{2+} ions by blue–green algae Spirulina sp.: Kinetics, equilibrium and the mechanism of the process. *Chemosphere* **2005**, *59*, 75–84. [CrossRef] [PubMed]
41. Franciski, M.A.; Peres, E.C.; Godinho, M.; Perondi, D.; Foletto, E.L.; Collazzo, G.C.; Dotto, G.L. Development of CO_2 Activated Biochar from Solid Wastes of a Beer Industry and Its Application for Methylene Blue Adsorption. *Waste Manag.* **2018**, *78*, 630–638. [CrossRef]
42. Wang, Y.; Liu, R. Comparison of Characteristics of Twenty-One Types of Biochar and Their Ability to Remove Multi-Heavy Metals and Methylene Blue in Solution. *Fuel Process. Technol.* **2017**, *160*, 55–63. [CrossRef]
43. Sen, A.; Pereira, H.; Olivella, M.A.; Villaescusa, I. Heavy metals removal in aqueous environments using bark as a biosorbent. *Int. J. Environ. Sci. Technol.* **2015**, *12*, 391–404. [CrossRef]
44. Wang, D.; Geng, Z.; Li, B.; Zhang, C. High Performance Electrode Materials for Electric Double-Layer Capacitors Based on Biomass-Derived Activated Carbons. *Electrochim. Acta* **2015**, *173*, 377–384. [CrossRef]
45. Angın, D.; Altintig, E.; Köse, T.E. Influence of Process Parameters on the Surface and Chemical Properties of Activated Carbon Obtained from Biochar by Chemical Activation. *Bioresour. Technol.* **2013**, *148*, 542–549. [CrossRef]
46. Hoslett, J.; Ghazal, H.; Mohamad, N.; Jouhara, H. Removal of Methylene Blue from Aqueous Solutions by Biochar Prepared from the Pyrolysis of Mixed Municipal Discarded Material. *Sci. Total Environ.* **2020**, *714*, 136832. [CrossRef]
47. Fan, S.; Wang, Y.; Wang, Z.; Tang, J.; Tang, J.; Li, X. Removal of Methylene Blue from Aqueous Solution by Sewage Sludge-Derived Biochar: Adsorption Kinetics, Equilibrium, Thermodynamics and Mechanism. *J. Environ. Chem. Eng.* **2017**, *5*, 601–611. [CrossRef]
48. Sahu, S.; Pahi, S.; Tripathy, S.; Singh, S.K.; Behera, A.; Sahu, U.K.; Patel, R.K. Adsorption of Methylene Blue on Chemically Modified Lychee Seed Biochar: Dynamic, Equilibrium, and Thermodynamic Study. *J. Mol. Liq.* **2020**, *315*, 113743. [CrossRef]